Impact of blood-brain barrier permeabilization induced by ultrasound associated to microbubbles on the brain delivery and kinetics of cetuximab: An immunoPET study using 89Zr-cetuximab

Vu Long Tran, Anthony Novell, Nicolas Tournier, Matthieu Gerstenmayer, Arnaud Schweitzer-Chaput, Claudia Mateos, Benoit Jego, Alizée Bouleau, Hervé Nozach, Alexandra Winkeler, et al.

Impact of blood-brain barrier permeabilization induced by ultrasound associated to microbubbles on the brain delivery and kinetics of cetuximab: an immunoPET study using ^{89}Zr-cetuximab

Vu Long Tran[1,+], Anthony Novell[1,+], Nicolas Tournier[1], Matthieu Gerstenmayer[2], Arnaud Schweitzer-Chaput[1], Claudia Mateos[1], Benoit Jego[1], Alizée Bouleau[1], Hervé Nozach[3], Alexandra Winkeler[1], Bertrand Kuhnast[1], Benoit Larrat[2], Charles Truillet[1,*]

+: co first authors. These authors have contributed equally to the experimental design and paper writing.

*: Corresponding Author.

charles.truillet@cea.fr

1- Université Paris-Saclay, CEA, CNRS, Inserm, BioMaps, Orsay, 91401, France

2- Université Paris-Saclay, CEA, CNRS, NeuroSpin/BAOBAB, Gif sur Yvette, 91191, France

3- SIMOS, CEA, Saclay, 91400 France

Abstract:

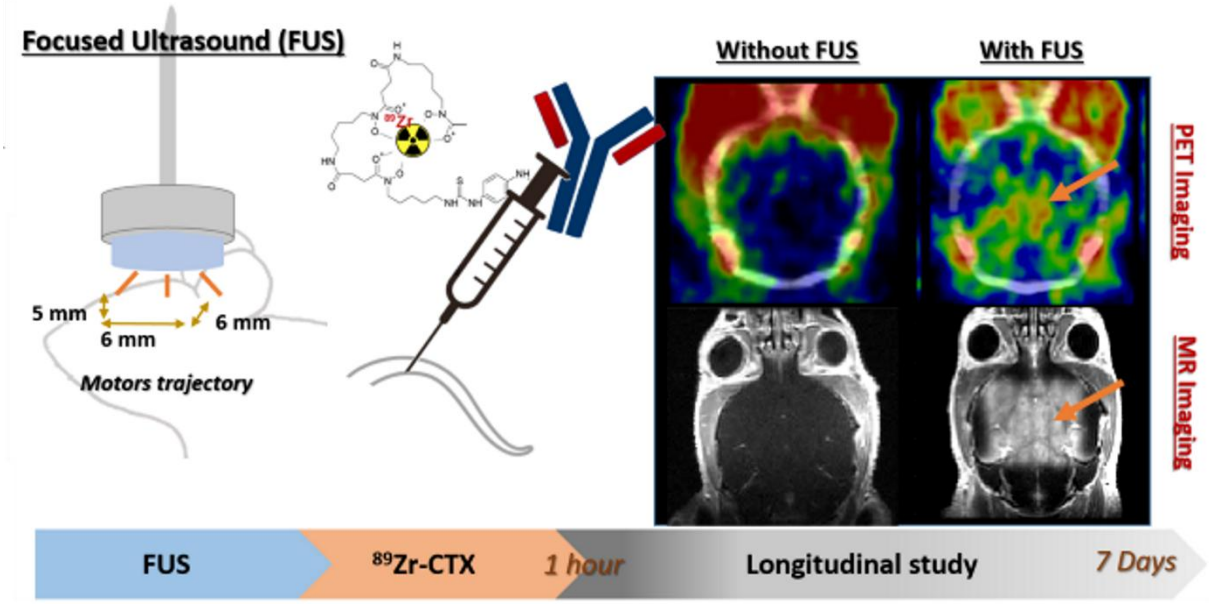

Abstract

Epidermal growth factor receptor (EGFR), involved in cell proliferation and migration, is overexpressed in ~50% of glioblastomas. Anti-EGFR based strategies using monoclonal antibodies (mAb) such as cetuximab (CTX) have been proposed for central nervous system (CNS) cancer therapy. However, the blood-brain barrier (BBB) drastically restricts their brain penetration which limits their efficacy for the treatment of glioblastomas. Herein, a longitudinal PET imaging study was performed to assess the relevance and the impact of focused ultrasound (FUS)-mediated BBB permeabilization on the brain exposure to the anti-EGFR mAb CTX over time. For this purpose, FUS permeabilization process with microbubbles was applied on intact BBB mouse brain before the injection of ^{89}Zr-labeled CTX for longitudinal imaging monitoring. FUS induced a dramatic increase in mAb penetration to the brain, 2 times higher compared to the intact BBB. The transfer of ^{89}Zr-CTX from blood to the brain was rendered significant by FUS (k_{uptake} = 1.3±0.23 min^{-1} with FUS versus k_{uptake} = 0 ±0.006 min^{-1} without FUS). FUS allowed significant and prolonged exposure to mAb in the brain parenchyma. This study confirms the potential of FUS as a target delivery method for mAb in CNS.

Key words: Antibody, pharmacokinetics, brain delivery, FUS, longitudinal PET imaging, Cetuximab, mAb diffusion.

Highlights:

- FUS and MB significantly increase the delivery of CTX across the BBB.
- PET is a powerful method to assess the PK of the passage of mAb through the BBB.
- ^{89}Zr-DFO-CTX was used to follow quantitatively enhanced brain exposure to CTX.
- ImmunoPET-combined FUS is a clinically relevant strategy for GBM innovative therapy.

I. INTRODUCTION:

Epidermal growth factor receptor (EGFR) plays a key role in essential cellular functions that include proliferation and migration. EGFR signaling mediates oncogenic progression and metastasis in several human malignancies including peripheral and CNS cancers such as glioma [1] [2]. *EGFR vIII* (deletions of exons 2-7) is the most prevalent mutation observed for EGFR. *EGFR vIII* is expressed in ~50% of glioblastomas which amplifies the expression of the wild-type protein [3]. Overexpression of EGFR is associated with poor prognosis in glioma patients [4]. The EGFR pathway is therefore regarded as a promising therapeutic target against CNS malignancies. In peripheral cancer, anti-EGFR monoclonal antibodies (mAb) were shown to inhibit cell proliferation, enhance apoptosis, and reduce angiogenesis, invasiveness and metastasis [5]. Anti-EGFR mAbs such as cetuximab (CTX) are active against EGFR vIII and prevent the binding of endogenous ligand [6]. Although anti-EGFR mAbs show favorable effects in colorectal, head and neck and non-small cell lung cancers, clinical trials using CTX in patients with glioblastoma did not show significant improvement over standard of care regimens [7,8]. The blood-brain barrier (BBB) is the main obstacle limiting the passage of therapeutics into the brain [9]. Insufficient exposure of CNS tumors to CTX across the BBB is widely assumed to explain the limited therapeutic efficacy.

For glioma, the abnormal tumor vasculature issued from the overproduction of proangiogenic factors leads to a compromised blood-tumor barrier (BTB) which is assumed to allow the extravasation of small and large molecules [10]. However, in reality, the penetration of drugs into the compromised BTB is very low, leading to inefficient tumor treatment. In early stages of glioblastoma (GBM), tumor own vasculature is not yet very well developed and the BTB is apparently not disrupted. At theses stages, BTB resembles the BBB and prevents efficient passage of cancer therapeutics, including small molecules and antibodies [11]. Moreover as glioma progresses, BTB presents some degree of heterogeneity i.e. all glioma have clinically significant regions of tumor with an intact BBB limiting the diffusion of treatment [12,13]. As mAb can be blocked from reaching the areas where the BBB remained intact, there is a clear need for strategies that can deliver immunotherapeutic agents into tumors.

The reigning paradigm to overcome this blockage shifted to the establishment of a safe and effective method to improve the brain delivery of mAb. Recent preclinical and clinical studies based on osmotic BBB disruption using intra-arterial mannitol infusion provided encouraging results in terms of improved drug delivery and safety, nevertheless these methods do not allow for controlled and localized BBB permeabilization [14]. The combination of injected microbubbles with low intensity focused ultrasound (FUS) is the most advanced method for controlled, minimally-invasive and transient BBB disruption in vivo [15–17]. Low acoustic pressures, produced by FUS, induce microbubble oscillations (alternation of expansion and shrinkage of microbubbles) near the vessel wall that can result in tight junction loosening due to local stress via push-pull mechanisms or microstreaming [18]. In preclinical model, FUS was recently shown to lead to a 3.5 fold increase in the brain concentrations of mAb [19]. However, current methods used to quantify drug concentrations in the brain are invasive or destructive (mass spectrometry, Elisa assay, HPLC). Non-invasive imaging technique such as magnetic resonance imaging (MRI) or positron emission tomography (PET) have therefore been developed to address the brain uptake of labeled mAbs, thus paving the way for the translational study of the neuropharmacokinetics of biologics [20,21]. However, to our knowledge, no *in vivo* imaging was proposed to study brain mAb concentrations over a prolonged time to provide an in-depth understanding of the neuropharmacokinetics and overall brain exposure to mAbs in vivo.

In the present study, the immunoPET paradigm was used to evaluate over time (up to 1 week) the impact of FUS-induced BBB opening on the delivery of CTX to the whole brain in mice with intact BBB. We used the long half-life ($t_{1/2}$ = 78.4 h) radionuclide zirconium 89 (^{89}Zr) which is relevant to the biological half-life of mAbs. In this work, kinetic modeling of the brain delivery of ^{89}Zr-CTX was performed to describe the initial transfer rate of CTX across the BBB and to address its retention by the brain over time.

We have found that FUS can increase significantly the uptake and the transfer rate of labeled mAb. Permeabilized ^{89}Zr-DFO-CTX stayed at the proximity of the FUS field for up to 72 h which further consolidate the rationale of using FUS as a controlled delivery method and ^{89}Zr PET imaging as a suitable monitoring technique.

II. MATERIALS AND METHODS

1. Materials

[^{89}Zr]Zr-oxalic acid was purchased from PerkinElmer (Netherlands). Erbitux (Cetuximab 5 mg/mL) was purchased from Merck (Belgium). p-isothiocyanatobenzyldesferrioxamine (p-NCS-Bz-DFO) was purchased from Chematech (Dijon, France). Ectodomain of human and murine EGFR was obtained from Sino Biological Inc. (Beijing, China). Sodium bicarbonate, sodium acetate, gentisic acid, dimethyl sulfoxide (DMSO) was purchased from Merck (Darmstadt, Germany). PD-10 desalting columns and iTLC-SG glass microfiber chromatography paper impregnated with silica gel were purchased from GE Healthcare (France). A431 and GL261 cells were obtained from DSMZ (Braunschweig, Germany). Fetal bovine serum (FBS) was purchased from PAA (Coelbe, Germany). L-glutamine, penicillin and streptomycin was obtained from Invitrogen (Frankfurt, Germany). *nu*/*nu* mice were purchased from Charles River (Écully, France). Microbubbles (SonoVue®) were purchased from Bracco (Milan, Italy). Gadoterate (Dotarem, about 1.66mmol/kg) was obtained from Guerbet (France).

2. CTX affinity for murine and human EGFR.

Binding kinetics of the interaction between CTX and the ectodomain of human and murine EGFR were determined using an Octet RED96 instrument (ForteBio). Anti-hIgG Fc Capture (AHC) Biosensors (Fortebio) were loaded with CRX using a 50 nM solution for 60 sec. After recording a 180 s baseline using a kinetic buffer (PBS buffer supplemented with 0.5% (*w*/*v*) bovine serum albumin (BSA) and 0.05% (*v*/*v*) Tween 20), the association of EGFR was measured at different concentrations for 200 s before a 2000 s dissociation step in kinetic buffer. Five concentrations of human EGFR ectodomain (25nM, 12.5 nM, 6.25nM, 3.125 nM, and 1.6 nM) and four concentrations of murine EGFR ectodomain (400 nM, 200nM, 100 nM and 50 nM) were tested. All measurements were performed at 25°C temperature in 96-well microplates. Data were analyzed using a 1:1 interaction model on the ForteBio data analysis software 10.

3. Radiolabeling of CTX with ^{89}Zr.

Cetuximab was radiolabeled with ^{89}Zr using p-NCS-Bz- (DFO) as chelate according to a previously described protocol.[22] Briefly, CTX (5 mg/mL) was dispersed in 200 µL of 0.1 M sodium bicarbonate buffer (pH 9.0). The final reaction mixture was adjusted to a total volume of 0.5 mL by adding 0.1 M sodium bicarbonate buffer. Four equivalents of DFO (in DMSO) were added to the antibody solution dropwise while mixing at 500 r.p.m. The reaction mixture was purified by running through a PD-10 column using sodium acetate containing gentisic acid as mobile phase (5 mg.mL^{-1} gentisic acid in 0.25 m sodium acetate (pH 5.4–5.6). Preparation of functionalized CTX (CTX-DFO) was stored at -20°C. On the day of imaging experiments, CTX-DFO was radiolabeled with ^{89}Zr (111 MBq) at 37°C for 60 min. ^{89}Zr-DFO-CTX was purified through PD-10 column using gentisic acid solution. The pH was carefully adjusted using a pH meter equipped with a micro pH electrode during the critical steps of the antibody functionalization and radiolabeling. For the radiolabeling, the pH was adjusted at 7.2 thanks to HEPES solution at 0.5M (Sigma, France) for optimal labeling efficiency. The radiochemical yield and purity were determined using instant thin- layer chromatography (ITLC) with iTLC-SG glass microfiber chromatography paper impregnated with silica gel as stationary phase and 20 mM citric acid (pH 4.9–5.1) as mobile phase. ITLC The migration was followed by radio- TLC detection (Mini-Scan TLC Imaging Scanner, Eckert&Ziegler,Berlin, Germany).

4. Cell cultivation

A431 cells (ATCC, CRL1555) and GL261 cells (DMZE, ACC 802) were cultured in DMEM high glucose (4500mg.L^{-1}) supplemented with 10% fetal bovine serum (FBS), GlutaMAX^{TM} (862 mg.L^{-1}), and 1% penicillin-streptomycin at 37 °C in a humidified atmosphere containing 95% air and 5% carbon dioxide (CO_2).

5. Functional Binding Assay of ^{89}Zr-DFO-CTX.

The immunoreactivity of the antibody for EGFR receptors after introduction of DFO and ^{89}Zr was assessed prior to any *in vivo* experiments. This assay was performed by a standard Lindmo excess antigen method involving the *in vitro* labeled CTX and EGFR overexpressing cells A431 [23]. These cells were established from a human epidermoid carcinoma expressing abnormally high levels of the EGFR. Briefly, 20 ng of radiolabeled CTX were added to 0.5–5x10^7 A431 cells in 0.5 ml of medium. Cells were incubated for 60 min at room temperature with continuous mixing throughout to keep them in suspension. Then, cells were harvested by centrifugation and washed once to remove unbound antibody, and pellets were measured in a gamma counter (Cobra II, Canberra-Packard, Schwadorf, Austria). The percentage of ^{89}Zr-DFO-CTX bound to A431 cells was calculated as the ratio of radioactivity in cell pellet to the mean total radioactivity associated with radiolabeled antibodies. The total applied radioactivity over specific bound radioactivity was plotted against the inverse of cell concentration. Fitting of a straight line to the data by means of linear regression analysis allows an easy and precise determination of the intercept value at the ordinate. This value is equal to the inverse of immunoreactive fraction of radiolabeled monoclonal antibodies.

The specificity of ^{89}Zr-DFO-CTX for human and murine EGFR antigen was tested using A431 cells and the mouse glioma cells GL261 that overexpresses murine EGFR. For each cell line, the incubation was performed either at a low concentration of ^{89}Zr-DFO-CTX alone (1 µg for 1x10^6 of cells, 1 µCi) or in the co-presence of a large excess of CTX (1000 µg for 1x10^6 of cells, 1 µCi)

6. Animal experiments.

Animal experiments have been performed using five-week old male *nu*/*nu* mice. They were conducted according to the European directive 2010/63/EU and its transposition in the French law (Décret n° 2013-118). Animal experiments were conducted at the imaging facility CEA-SHFJ (authorization D91-471-105/ethics committee n°44). Mice were housed in standard conditions (microisolator polycarbonate cages, aspen wood as bedding material, 4 mice in each cage, room temperature 22°C, humidity 40%) under a regular 12-hour dark/light cycle. Animals were fed with standard nutritional cubes. Food and water were available ad libitum. Mice were provided with clean shredded papers or cotton square nestles as nesting materials, and polycarbonate cottages and wooden sticks as environmental enrichments. Animals experiments were performed under isoflurane anesthesia (2.5 – 3% isoflurane in oxygen for induction and 1 – 2 % isoflurane in oxygen for maintenance. The level of oxygen flow that we used was in the range of 1.5 – 2 l.m^{-1}). In total, 32 mice were used for this study. Mice were separated randomly into different groups. More details are described in the study design ^{89}Zr-DFO-CTX PET experiments. Experimenters were blinded with mice's identity during administration and imaging procedures.

7. *In vivo* stability of ^{89}Zr-DFO-CTX.

Blood samples were obtained from the tail vein 1 h and 48 h after *iv* injection of ^{89}Zr-DFO-CTX or left ventricle via cardiac puncture 7 days after *iv* injection of ^{89}Zr-DFO-CTX. They were immediately centrifuged at 2300g for 15 min at 4 °C. During the whole process, mice were kept under anesthesia or deep terminal anesthesia (for cardiac puncture). Radioactivity of the supernatant was immediately resolved by ITLC allowing separating ^{89}Zr-DFO-CTX from ^{89}Zr or ^{89}Zr-DFO. The experiments were done in triplicate.

8. **FUS-induced BBB permeabilization.**

Permeabilization of the BBB was achieved using a focused transducer (active diameter 25 mm, focal depth 20 mm, Imasonic, Voray sur l'Ognon, France) centered at 1.5 MHz connected to a single-channel programmable generator (Image Guided Therapy, Pessac, France). The transducer has an axial and a lateral resolution of 5 mm and 1 mm, respectively. The beam profile was measured using a calibrated hydrophone (HGL-200, Onda Corporation, CA, USA). Reported values corresponded to the width and the length at 6 dB. The transducer was mounted on a motorized XYZ-axis stage and positioned above the mouse head maintained under anesthesia. The device was coupled to the mouse skull using a latex balloon filled with deionized and degassed water and coupling gel. The distance between the transducer and the skull was adjusted by the displacement of the motorized axis (Z) and the filling of the balloon in order to get the center of the brain at the focal distance (i.e., 20 mm). Typically, for transcranial BBB opening in human, a lower frequency (<0.4 MHz) is chosen to limit the attenuation of the skull. In that case, the axial resolution is about few cm while lateral resolution is about few mm. The clinical transfer of FUS-mediated BBB opening for GBM therapy is currently under investigation.

A 50 µL bolus of microbubbles (SonoVue®, Bracco, Milan, Italy, 1.5×10^8 microbubbles/mL) were intravenously administered in the tail vein. A mechanical zig-zag shaped scan (XY-axis) was synchronized to the generator output in order to induce a wide BBB opening covering a square region in the middle of the brain of 6 mm x 6 mm in order to open a large area of the mousse brain including the two hemispheres but excluding the cerebellum. Motor speed was set to 10mm.s-1 and the time trajectory was 5.1 s. Ultrasonic waves were continuously transmitted at 1.5 MHz during the transducer translation. However, to avoid an excessive deposit of ultrasound energy at a focal spot, FUS was briefly turned off during the changes of direction in the mechanical scan. This results in a final duty cycle of 69%. The sequence was repeated 25 times for a total exposure of 127 s. The transmitted in situ peak negative pressure in the mouse brain is estimated to be 430 kPa (520 kPa in deionized water) considering a skull attenuation of 18% (average value of the skull attenuation measured in Choi et al [24]) at 1.5 MHz.

This protocol was optimized for C57BL/6 mice in a previous study. The FUS safety on nude mice was also assessed during this study.[25] Here, we first validated the acoustic parameters on 6 nude mice using contrast enhanced MRI as biomarker of BBB integrity. With this aim, mice were iv injected (tail vein) with 100µL of gadoterate (about 1.66mmol/kg, Dotarem, Guerbet, France) right after sonication ended. Mice were immediately placed inside a small animal 7T MRI (Bruker, Germany) and T1-weighted images were acquired according to following parameters: Multi Slice Multi Echoes, TE 5 ms, TR 300 ms, resolution 0.15x0.15x0.4 mm3, matrix size 128x128x20, 8 averages, total acquisition time = 5 min. Effective BBB disruption was confirmed by the enhancement of the T1-weigted signal due to gadolinium leakage within the square shaped sonicated region. No side effect (edema, bleeding) were observed and the distribution of gadolinium was homogeneous in the targeted area.

9. **Study design of ^{89}Zr-DFO-CTX PET experiments.**

Four groups of mice (Nu/Nu mice, 5 weeks, male) were studied: (i) the sham group, with no FUS BBB opening and microdose (10 µg/mouse) of ^{89}Zr-DFO-CTX (high specific activity, i.e the ratio between radioactivity and injected mass of mAb). This sham group was used to assess the brain kinetics of 89Zr-DFO-CTX when the BBB is intact. These animals received the microbubble injection and a sham FUS protocol with zero ultrasound amplitude. (ii) FUS group. Permeabilization of the BBB was achieved with the validated FUS protocol and microdose of ^{89}Zr-DFO-CTX (high specific activity, 10 µg/mouse) injected 10 min after FUS. The tracer was injected after FUS protocol in order to obtain the entire kinetics of mAb from the time of injection till 7 days after injection. (iii) The pharmacologic dose (PD, 1mg of unlabeled CTX per mouse was added) group, without FUS BBB opening and low specific activity. This group allows determining the impact of CTX diffusion into the healthy brain with high dose of CTX mimicking the pharmacologic situation. (iv) FUS pharmacologic dose group with FUS-induced BBB permeabilization co-injected with a target- pharmacologic dose ^{89}Zr-DFO-CTX (low specific activity, 1mg per mouse) (Fig. SI1.).

10. **PET acquisition.**

PET acquisitions were performed using a Siemens Inveon small animal PET scanner associated to a CT scanner (Knoxville, TN, USA). The catheter inserted in the tail vein for injection of microbubbles (50 µL) was then used for injection of ^{89}Zr-DFO-CTX. The injection of ^{89}Zr-DFO-CTX (in <150µL saline solution) was performed 10 min after FUS under the PET scanner. All groups received similar doses of radiolabeled ^{89}Zr-DFO-CTX (0.24 ± 0.07 MBq/g). A 60 min dynamic PET acquisition was first performed immediately after injection of the ^{89}Zr- DFO-CTX. Then, at selected time points after injection (4h, 24h, 48h, 72h and 7 days after the injection), mice were anesthetized and installed under the PET scanner for a 30 minute static PET acquisition. All the mice (n=8) were imaged at all the time points, except for the FUS groups (microdose and pharmacologic dose) at 4 hours (n=6).

11. **PET images reconstruction and analysis.**

The spatial resolution of the PET scanner is ~1.5 mm (FWHM). PET images were reconstructed using a 2D-OSEM iterative algorithm. Volumes of interest (VOI) were delineated manually based on CT images on sonicated/non-sonicated brain regions and the heart-blood pool on summed PET images using PMOD software (Version 3.9, Switzerland) and Carimas (Turku PET Centre, Finland). All the images and extracted data were corrected according to the half-life of ^{89}Zr in order to obtain the accurate uptake in each organ. Time-activity curves (TACs) were generated from each VOI to describe the kinetics of ^{89}Zr-DFO-CTX. The activities were expressed as the percentage of injected dose per volume (%ID/cc). The area under the TACs (AUC) from time 0 to 60 min for the dynamic scan was calculated to describe the organ exposure to CTX (GraphPad Prism). The total volume of distribution (V_T, mL.cm^{-3}) defined as the ratio of the radioligand concentration in the tissue of interest to that in the blood at equilibrium was estimated using the Logan graphical method.[26] V_T encompasses both the BBB permeation and the total binding of ^{89}Zr-DFO-CTX to the brain. Estimation of V_T was not possible in two mice that show large movement due to respiration, which made it impossible to get accurate blood function.

12. **Integration Plot Analysis.**

Integration plot analysis was used to graphically estimate the uptake transfer of ^{89}Zr-DFO-CTX from blood to plasma ($k_{uptake,brain}$) across the BBB, as previously described.[27] The uptake from blood to brain was calculated by the integration plot method using the portion of time profile of the radioactivity during which brain radiotracer excretion from the blood or other organs was negligible (between 15s to 3min). Similar to V_T estimation, the $k_{uptake,brain}$ was not estimated in two mice that present large heart movement due to respiration. Mathematical models for Logan plot and integration plot were provided in more details in the Supplementary Information.

13. **Statistics.**

All data are presented as mean ± standard deviation. The statistical analyses were performed using GraphPad Prism software (Graph Pad software Inc., San Diego, USA). Comparisons of PET data between FUS and Non FUS over time were performed using a one-way ANOVA. Changes at the 95% confidence level ($P < 0.05$) were qualified as statistically significant.

III. RESULTS

1. The relevance of using CTX in a mouse model for assessing the effect of FUS to increase mAb diffusion through BBB.

Correct interpretation of the brain kinetics of a mAb requires information regarding its specific and/or nonspecific binding to target tissues. CTX is a chimeric monoclonal antibody where the variable regions of immunoglobulins have a murine origin [28]. Previous studies suggested a low binding on murine EGFR, specifically with NMRI mouse by competitive binding assays [29]. However, binding kinetic constants in a direct binding assay remained to be determined. K_D of CTX for human EGFR was measured at 950 pM for human EGFR, approximately ~70 times higher than for murine EGFR (K_D = 65 nM) (Fig. 1A and B). Binding assays on human (A431) and mouse (GL261) cells expressing high level of EGFR were also conducted using the radiolabeled compound ^{89}Zr-DFO-CTX. Before the

assays, to control that the radiolabeling process does not strongly affect the affinity of CTX for human EGFR, the immunoreactive fraction of ^{89}Zr-DFO-CTX was also measured on A431 cells at infinite antigen excess. The immunoreactive fraction was determined to be close to 100% (Fig. 1C). The results of binding assays also showed low uptake of CTX for mouse GL261 cells and high uptake for human A431 cells (Fig. SI2). Moreover, the binding of CTX to A431 cells is displaceable whereas the binding of CTX to GL261 cells is non-displaceable.

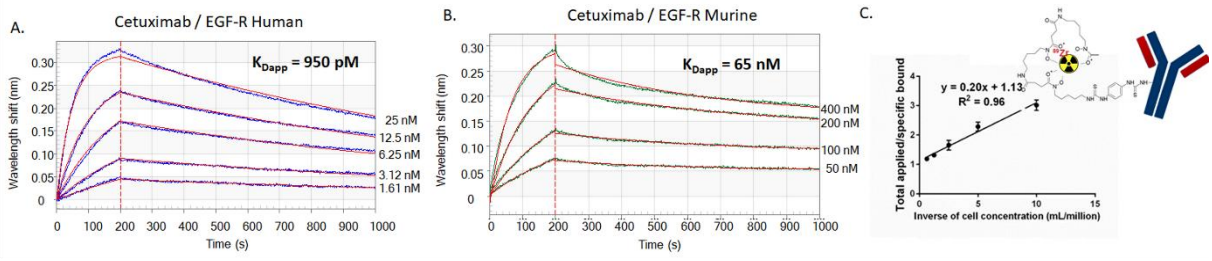

Figure 1. The kinetic rate constants of CTX for human EGFR and murine EGFR. Kinetic rate constants of interaction between CTX and human EGFR ectodomain (**A**) or murine EGFR ectodomain (**B**) were determined using BioLayer Interferometry. **C.** The immunoreactive fraction of ^{89}Zr-DFO-CTX was measured by performing a linear regression analysis of a plot of (total/bound) activity versus (1/[concentration of cells]) yielding the immunoreactive fraction determined as 1/y-intercept.

2. **FUS enabled the BBB permeation of ^{89}Zr-DFO-CTX.**

Firstly, T_1-weighted MRI after the injection of gadoterate was performed to validate the procedure for FUS-induced permeabilization of the BBB (Fig. SI3 A.). The result showed a persistent contrast enhancement in the sonicated brain area.

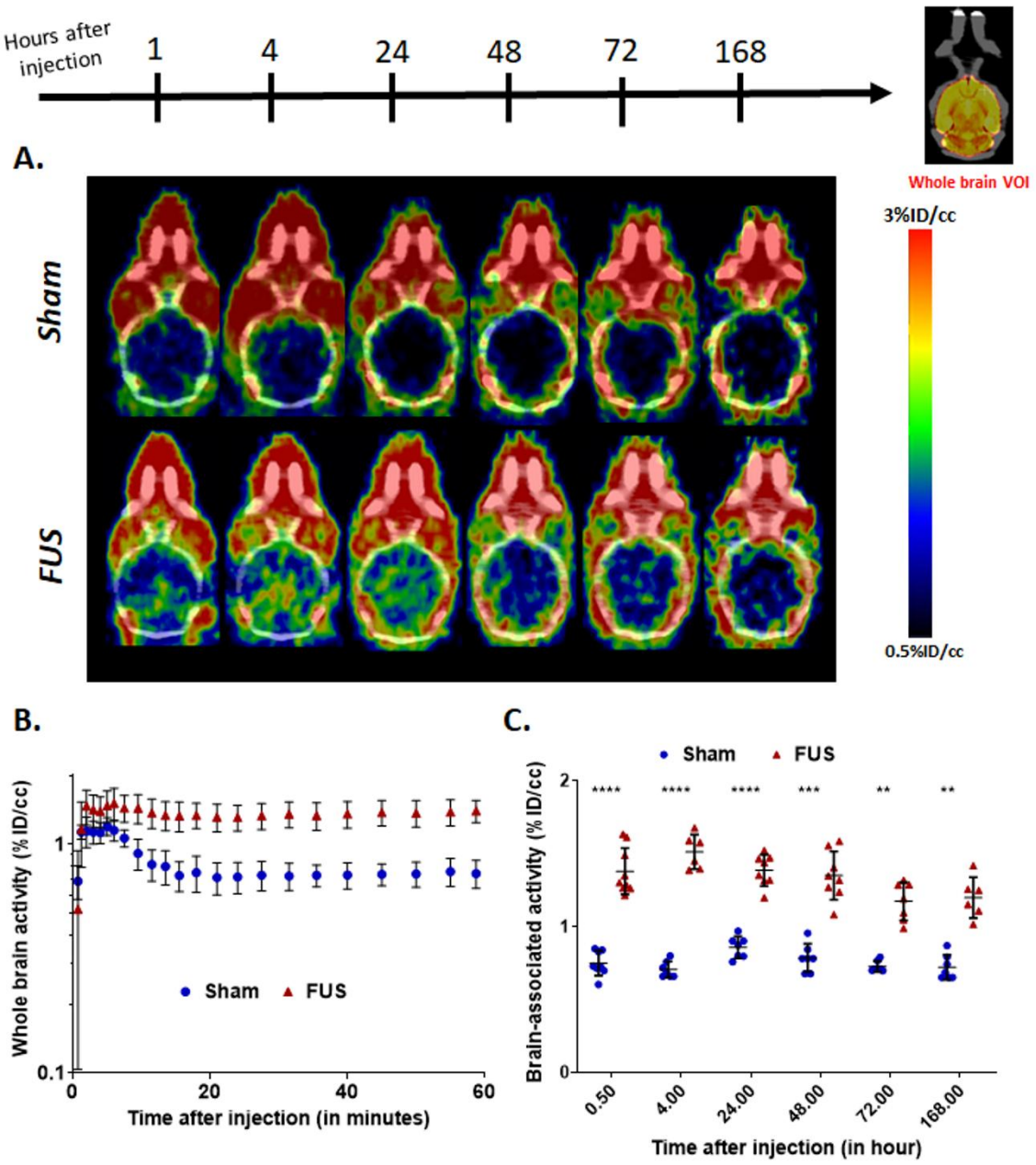

Figure 2. Brain kinetics of ^{89}Zr-DFO-CTX after FUS-induced BBB permeabilization. (A) Representative PET images obtained from the same mouse at different time points (1 h, 4 h, 24 h, 48 h, 72 h and 168 h after injection) for the *sham* (top) and the FUS (bottom) groups. Time-activity curves (TACs) in the whole brain of ^{89}Zr-DFO-CTX injected to sham group (blue) and FUS group (red) group during 60 min **(B)** and up to 168 h **(C)** (n=8 for each group). Data were extracted from a whole brain volume of interest (VOI, represented by a yellow color zone inside the skull). Statistical significance was determined using unpaired *t* tests with * $p<0.05$, ** $p<0.01$, *** $p<0.001$, **** $p<0.0001$. All data are represented as mean ± SD. No statistical significance was observed for the sham group, at any time after injection. Sagittal images are in FigSI3.B.

Then, the same protocol of FUS was applied before the injection of ^{89}Zr-DFO-CTX. FUS protocol does not have an impact on the overall distribution of ^{89}Zr-DFO-CTX except on the brain area where FUS was applied (Fig. SI9). We have found that BBB permeabilization enabled by FUS significantly enhanced the brain uptake of ^{89}Zr-DFO-CTX (Fig. 2A and B). The initial accumulation of ^{89}Zr-DFO-CTX in the brains of FUS group was higher than in the sham group as early as 15 min after the injection of labeled compound. Maximal brain concentration (C_{max}) occurred at 4 hours after injection.

The maximal brain concentration of ^{89}Zr-CTX in the brain without FUS was 0.70 ± 0.06 %ID/cc, which corresponds to the vascular content. The brain concentration of ^{89}Zr-CTX in FUS-treated animals was significantly higher and maximal after 4h (1.51 ± 0.12 %ID/cc, p<0.001). The activity at the plateau after BBB permeabilization was almost two times higher than the one obtained in the *sham* group. The difference between two groups remained significant even up to 168 h post injection (Fig. 2C).

On the other hand, metabolic stability of ^{89}Zr-DFO-CTX was assessed in plasma samples obtained at 1 hour, 48 h and 168 h post FUS. No release of DFO-^{89}Zr, free ^{89}Zr, or other radiolabeled fragments could be observed (Fig. SI4).

3. Modeling ^{89}Zr-DFO-CTX brain kinetics to elucidate the impact of BBB disruption on mAb delivery into the brain.

Besides giving the concentration of radioactivity (%ID/cc) in tissue, our dynamic PET images also allow estimating the total volume of distribution (V_T) and the uptake kinetic constant (k_{uptake}). We have found that the concentration of radioactivity in the brain at 24h post-injection was significantly correlated with the V_T estimated in the first 60 min post injection from dynamic data ($P < 0.0001$; $r^2 = 0.94$). This correlation included animals of the sham, pharmacologic dose sham, FUS and pharmacologic dose FUS groups (Fig.3A). A significant correlation was also observed between brain V_T and brain AUC ($P<0.0001$, $r^2 = 0.92$) as shown in (Fig. SI5). Both parameters were estimated from dynamic data obtained from 0 to 60 min post injection.

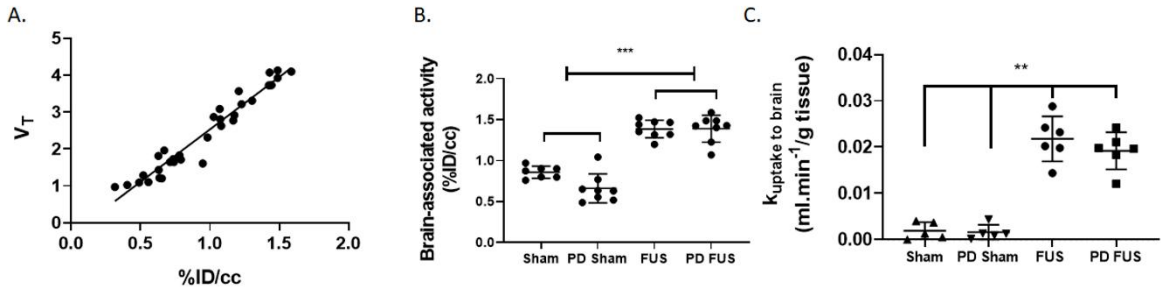

Figure 3. Comparison of PET imaging quantification between different groups and pharmacokinetics calculation. A. Correlation between V_T and the concentration of activity (%ID/cc) at 24 h post-injection. **B**. Concentration of activity in the brain 24 hours after injection in different groups (sham, pharmacologic dose (PD) sham, FUS and pharmacologic dose (PD) FUS). **C**. Brain uptake transfer (k_{uptake}) of ^{89}Zr-DFO-CTX in different groups. **P<0.01, n=8 mice per group.

The assumption of equivalent nonspecific binding is usually evaluated *in vivo* with the displacement of radiotracer binding by high doses of a nonradioactive drug, called a pharmacologic dose [30]. Thus, to confirm that specific binding does not account for ^{89}Zr-DFO-CTX brain distribution, we compared the brain kinetics of microdose ^{89}Zr-DFO-CTX (low amount of CTX included in the radiotracer injection dose) with a pharmacologic dose (radiolabeled CTX co-injected with a large amount of unlabeled CTX) in different conditions (Sham and FUS). No difference on the tracer uptake was observed between the microdose and the pharmacologic dose condition (sham: 0.85± 0.07% ID/cc vs pharmacologic dose: 0.67±0.18% ID/cc and FUS: 1.38 ± 0.11% ID/cc vs FUS pharmacologic dose: 1.39 ± 0.16 %ID/cc). Fig 3.B. The V_T of ^{89}Zr-DFO-CTX in brains of different groups, derived from the dynamic PET imaging (first hour after injection) corroborated this result (Fig SI6). Since the ^{89}Zr-DFO-CTX uptake in the whole brain was not affected by the pharmacologic dose displacement assay, ^{89}Zr-DFO-CTX was not impacted by murine EGFR expression. To confirm this in vivo observation, on nu/nu brain mice frozen slice, *in vitro*, ^{89}Zr-DFO-CTX and fluorescent CTX were incubated. Neither radioactive signal nor fluorescent signal were observed (FigSI10).

The rate constant for the transfer of radiotracer from the blood to the brain (k_{uptake}), which was calculated based on the integration plot analysis from the initial brain uptake of the radioactivity, shortly after the injection, was significantly higher in the FUS group ($13x10^{-3} \pm 6x10^{-3}$ $ml.min^{-1}.g^{-1}$) than in the sham group ($29.3x10^{-6} \pm 15x10^{-6}$ $ml.min^{-1}.g^{-1}$). No significant difference of transfer rate was observed between pharmacologic dose and the microdose groups.

4. **Slow diffusion of ^{89}Zr-DFO-CTX within the brain parenchyma.**

Longitudinal imaging study was performed for several days after FUS-induced BBB permeabilization to investigate the diffusion of ^{89}Zr-DFO-CTX from the sonicated area to the brain parenchyma. A threshold was applied into the PET images to suppress the background and facilitate the determination of the volume of ^{89}Zr-DFO-CTX accumulation in the brain after BBB permeabilization (Fig. 4A). The threshold that was chosen corresponds to the mean of the concentration of activity (%ID/cc) in the cerebellum plus two times the standard deviation. The cerebellum region was used as the region of reference since no FUS was applied on this region. Indeed, the uptake in the cerebellum remains constant over time (Fig. SI7). In order to quantify the diffusion of mAbs over time, the activity of the defined (by the threshold) volume was compared to the activity of the whole brain volume (Fig. 4B).

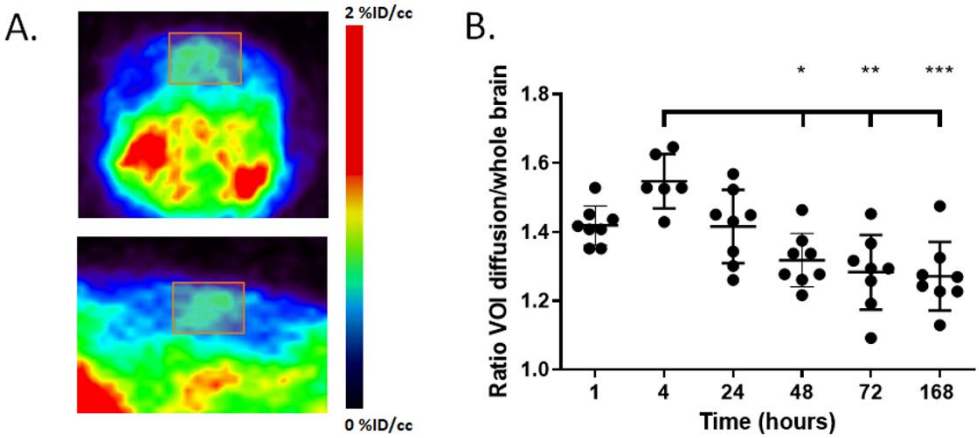

Figure 4. ^{89}Zr-DFO-CTX diffusion within the brain after FUS-mediated BBB opening. **A.** PET images showing the delineation of radiolabeled CTX four hours after FUS-induced BBB permeabilization. The box in orange indicate the area of the threshold applied to delimitate the brain parenchyma where was applied the FUS **B.** Ratios between the activities onto the VOI defined at four hours and the whole brain activity at different times. Significant differences were observed between 4 hours and 48, 72 and 168h (*p<0.05, **p<0.01, ***p<0.001, n=8 mice per group).

In each individual animal, the elimination half-life of ^{89}Zr-DFO-CTX from the sonicated brain tissue was calculated by fitting the time decay of the activity with an exponential function. Brain $T_{1/2}$ was determined to be in average equal to 21.4±1.7h. Meanwhile, the elimination half-life from blood was calculated using the blood activity over time $T_{1/2}$ = 5.7±0.4h. In sham animals, the elimination half-life of ^{89}Zr-DFO-CTX from brain was 5.01±0.7h, consistent with the blood $T_{1/2}$ = 6.3±0.2h.

After FUS was applied, the amount of ^{89}Zr-DFO-CTX in the brain remained stable, with a slight decrease after several days. The ratio of radioactivity measured in the sonicated region to the whole brain was maximal at 4 hours after the injection and then slowly decreased down to 1.27±0.10, 168 hours after the injection. This suggests a limited and slow diffusion of ^{89}Zr-DFO-CTX from the sonicated area to the surrounding brain region and a limited clearance of ^{89}Zr-DFO-CTX from the targeted tissue, allowing for high and localized exposure.

IV. DISCUSSION

EGFR is one of the major target for cancer therapy in a large variety of cancers [31]. Despite some promising studies proposing EGFR-targeting therapies such as small molecule tyrosine kinase inhibitors or mAbs with CTX, the potential of these agents against glioblastoma has been unfulfilled [32]. One of the reasons for the resistance of glioblastoma cells to treatments might be the limited diffusion of molecules in general and biologics in particular across the BBB that has been underestimated. Till recently, it has been taken for granted that the presence of glioblastoma tumors induced an obvious physical disruption of the BTB in patients [33,34]. To our knowledge no clinical trials have explored or even tried to predict the ability of mAb to reach the tumors as a factor of response in patients with glioblastoma. A limited number of groups have indirectly suggested a link between mAb efficacy and BBB integrity in preclinical studies [9,35]. In this context, FUS has emerged as a clinical mean to increase the permeability across the BBB to therapeutics including mAbs. From the initial studies where high-intensity FUS was applied to increase the permeability of mAb into subcutaneous tumors,[36] newer strategies have evolved where the combination with microbubbles administration help reduce the required intensity of FUS and induce a greater permeabilization capacity. Such mild approach might be safer, more suitable for delicate tissues and appears to be efficient for BBB. A total of six trials have been or are currently conducted on GBM patients using a variety of devices including SonoCloud® (CarThera), ExAblate® (InSightec), and NaviFUS® (NaviFUS cooperation), both with and without chemotherapy regimens (for clinical safety), such as carboplatin, doxorubicin and temozolomide[37]. However, only few noninvasive methods have been explored to characterize FUS-enhanced mAb delivery through the BBB in a translational perspective. Fluorescent antibody-based ligands have been developed to characterize FUS-mediated mAb delivery and demonstrate that this technique is valuable to monitor antibody delivery.[38] However, fluorescence imaging is difficult to translate into clinic due to the poor tissue penetration of light. In this aspect, PET imaging is superior to fluorescence imaging thanks to much higher penetrability of gamma ray. Hence, it offers a sensitive, dynamic and quantitative imaging modality to investigate the distribution of mAb in the whole-brain parenchyma after FUS-induced permeabilization of the BBB. Therefore, PET imaging has more potential to be transferred to clinical trials in a rather straightforward manner. Several groups are currently using this so-called immunoPET technique for peripheral tumor imaging in clinical trials [39,40]. ImmunoPET is expected to become widespread in the future due to the increase of immunotherapy strategies around the world. This molecular imaging technique could improve drastically the efficacy of treatment by monitoring quantitatively the efficacy of drug delivery as well as to visualize the distribution of predictive biomarkers in deep-seated organs and/or in a large area, or even in whole-body scale.

It is to our knowledge the first study to clarify the kinetic impact of FUS on the BBB crossing and diffusion of mAb in the brain parenchyma. The use of translational imaging paves the way for the use of PET with radiolabeled mAb (^{89}Zr-DFO-CTX in this particular case) to address the neuropharmacokinetic correlation of the efficacy of mAbs in brain tumors. This approach will be useful to provide the proof-of-concept on the potential of FUS to enable molecularly targeted immunotherapy against CNS tumors with intact BBB.

According to the Allen Brain Atlas and to Estrada *et al*., low EGFR expression was found in the brain of healthy mice [41]. Endogenous expression of murine EGFR in brain is therefore not likely to account for ^{89}Zr-DFO-CTX binding to the brain. We have shown that CTX and ^{89}Zr-DFO-CTX have low affinity for the murine epitope, that have been already described by different groups [42]. Moreover, the displacement in vivo assay with the pharmacological dose prove the non-specificity of ^{89}Zr-DFO-CTX for murine EGFR expression. ^{89}Zr-DFO-CTX kinetics therefore predominantly reflect the mechanical uptake of the compound across BBB rather than its binding.

The BBB is a unique and highly selective barrier composed of cerebral endothelial cells tightly connected to each other by tight junctions and adherent junctions [43]. Intact BBB limits the brain penetration of antibodies from the systemic circulation [35]. Typically, antibody concentrations are 1,000 times lower in the brain than in the bloodstream. Moreover, the low passage of mAb through the

intact BBB is a slow phenomenon [44]. ^{89}Zr-DFO-CTX PET images in *sham* animals confirmed the negligible permeation of CTX across the intact BBB. After FUS treatment, we clearly show a drastic increase in the uptake of ^{89}Zr-DFO-CTX in the sonicated brain area (two times compared to the intact BBB brains in the sham group). The accumulation was maximum during the first hours right after the FUS opening. The BBB closure is a progressive process. Small particles (< 1nm) are able to pass through the BBB for hours while the passage of large particles (>50 nm) is limited to few seconds. Conti et al. have presented a mathematical model able to predict the evolution time of drugs concentration in the function of their size after BBB permeabilization by FUS [45]. According to this study, mAbs (around 150 kDa) should be able to cross the BBB only during the first 15 minutes after FUS was applied since the disruption of tight junction is only transient. This model assumes that molecular size is the only parameter directing BBB crossing while other properties can explain deviations from this model: molecule anisotropy, lipophilicity, surface charge, active transport [46]. Furthermore, even if the mean tight junction size is expected to be smaller than CTX size very fast after US, a limited number of junctions will remain open for this size for much longer time and could explain our results since CTX circulates for a long time.

The transfer rate characterizing the passage of mAb through the BBB was boosted up to 2 $mL.min^{-1}.100gr^{-1}$ right after BBB opening from almost zero without BBB opening. Making the best with the long physical decay of ^{89}Zr, the elimination half-life of ^{89}Zr-DFO-CTX from the sonicated brain tissue ($T_{1/2}$ = 21.4±1.7h) was significantly different from the elimination half-life from blood (($T_{1/2}$ = 5.7±0.4h). Elimination from the sonicated brain was significantly slower, which confirmed the retention of ^{89}Zr-DFO-CTX in the targeted tissue. In *sham* animals, the elimination half-life from the blood and from the brain were similar, thus suggesting that the intact BBB brain radioactivity mainly reflected the vascular content of the brain compartment.

The brain concentration of ^{89}Zr-DFO-CTX (in %ID/cc) are tightly correlated to the brain V_T, which considers the blood radioactivity kinetics. The V_T of ^{89}Zr-DFO-CTX in the brain therefore provides a more precise parameter to describe the distribution of the mAb to the brain parenchyma over time. This strong correlation between V_T and brain activity suggest that FUS does not affect the blood kinetics and metabolism of ^{89}Zr-DFO-CTX as well as the vascular content of the brain compartment.

Two different concentrations of CTX, 10 µg/mouse and 1 mg/mouse were tested for every condition (without and with BBB opening). We observed no difference in the overall uptake of ^{89}Zr-DFO-CTX by the brain between the low dose (10 µg/mouse) and the pharmacologic dose (1 mg/mouse) whatever the status of BBB integrity was. CTX has low affinity for mouse EGFR that suggests a limited binding of ^{89}Zr-DFO-CTX to the mouse organs. This observation suggests that the uptake did not depend on the ^{89}Zr-DFO-CTX / CTX ratio in the blood-pool. It was confirmed by the transfer rate which has neither been modified at the low dose nor at the pharmacologic dose. The BBB is, therefore, the main determinant of the brain kinetics of CTX. The brain distribution of mAb therefore reflects the extravasation and elimination processes driven by the convective lymph flow to and from the tissue, and the vascular and interstitial reflection coefficients. This observation has been suggested by other groups [47,48]. The microdose ^{89}Zr-DFO-CTX therefore predicts the pharmacologic situation and can be safely used in clinical trials to study the brain kinetic of CTX.

We show that the amount of ^{89}Zr-DFO-CTX delivered to the sonicated area only slowly diffuses throughout the brain parenchyma, suggesting appreciable accumulation of the mAb in the targeted region. This result is consistent with the expected typical passive diffusion of CTX in the extracellular compartment according to its estimated molecular size. In the first hours after the injection, there was a slight local diffusion and accumulation of labeled CTX right below the center zone where FUS was applied. After 24 hours, there was a slow but significant release of the radioactivity from the sonicated area to the surrounding brain tissue demonstrated by a gradual decrease of the ratio between the activity in the locally-diffused VOI and the one in the whole brain. Moreover, the CTX seems to be slightly decreasing overtime taking into consideration the global brain uptake. This CTX elimination may be explained by the lymph turnover process involved in the brain [49]. This means that once BBB integrity is restored, CTX action will be restricted to the FUS area where it entered brain parenchyma.

Limited penetration and the associated steep concentration profiles of mAb in function of distance into the brain after local delivery were already well documented [50]. Wolak et al. have shown that IgG antibody diffusion in brain extracellular space is limited compared to in free solution by nearly one order of magnitude. The extracellular distribution in brain tissue is significantly hindered [50]. In addition, Silburt et al. have shown that FUS perturbation seems to have a little influence on biologic flow through the brain. But this effect still remains limited without inducing a large change in the diffusion properties of the brain cortical space [51].

V. CONCLUSION

Our results show the impact of FUS-induced transient BBB permeation on the delivery of CTX across the BBB and subsequent brain exposure. To this end, we used pharmacokinetic in vivo imaging making the best from quantitative capacity of PET and long half-life ^{89}Zr labeled CTX. FUS induced a drastic increase in the penetration of CTX to the brain followed by a low diffusion of the mAb within the brain parenchyma. Our results show the relevance for FUS technology to enable sufficient and targeted exposure of the brain tissue to mAbs. In this context, FUS may ultimately provide a relevant and realistic technique to enable CNS targeted immunotherapy, especially with anti-EGFR treatment. This complete study is the essential first step to further discriminate between BTB and BBB to improve FUS mAb delivery in GBM environment. Further experiments are needed to test whether this technique can significantly improve the delivery of ^{89}Zr-DFO-CTX in GBM orthotopic models with different levels of BTB disruption and BBB integrity. Malignant tissue might present, to some extent, similarity to healthy brains as well as some disparity in terms of physiology and biology. In view of such a broad prospective, this work hopefully provides another strong evidence to pave the way for more investigations into this exciting field.

COMPETING INTERESTS

The authors have declared that no competing interest exists

ACKNOWLEDGEMENTS

This work was supported by CEA (program Bottom-up) and the Research Foundation Against Cancer, ARC.

ABBREVIATIONS

EGFR: epidermal growth factor receptor; CTX: cetuximab; mAb: monoclonal antibody; BBB: blood brain barrier; CNS: central nervous system; BTB: blood-tumor barrier; FUS: focused ultrasound; MRI: magnetic resonance imaging; PET: positron emission tomography; DFO: Deferoxamine; iTLC: instant thin- layer chromatography, ^{89}Zr: Zirconium-89Zr.

REFERENCES

[1] S. Sigismund, D. Avanzato, L. Lanzetti, Emerging functions of the EGFR in cancer, Mol. Oncol. 12 (2018) 3–20. https://doi.org/10.1002/1878-0261.12155.

[2] T. Mitsudomi, Y. Yatabe, Epidermal growth factor receptor in relation to tumor development: EGFR gene and cancer, FEBS J. 277 (2010) 301–308. https://doi.org/10.1111/j.1742-4658.2009.07448.x.

[3] R.G.W. Verhaak, K.A. Hoadley, E. Purdom, V. Wang, Y. Qi, M.D. Wilkerson, C.R. Miller, L. Ding, T. Golub, J.P. Mesirov, G. Alexe, M. Lawrence, M. O'Kelly, P. Tamayo, B.A. Weir, S. Gabriel, W. Winckler, S. Gupta, L. Jakkula, H.S. Feiler, J.G. Hodgson, C.D. James, J.N. Sarkaria, C. Brennan, A. Kahn, P.T. Spellman, R.K. Wilson, T.P. Speed, J.W. Gray, M. Meyerson, G. Getz, C.M. Perou, D.N. Hayes, Cancer Genome Atlas Research Network, Integrated genomic analysis identifies clinically relevant subtypes of glioblastoma characterized by abnormalities in PDGFRA, IDH1, EGFR, and NF1, Cancer Cell. 17 (2010) 98–110. https://doi.org/10.1016/j.ccr.2009.12.020.

[4] A. Shergalis, A. Bankhead, U. Luesakul, N. Muangsin, N. Neamati, Current Challenges and Opportunities in Treating Glioblastoma, Pharmacol. Rev. 70 (2018) 412–445. https://doi.org/10.1124/pr.117.014944.

[5] Z. An, O. Aksoy, T. Zheng, Q.-W. Fan, W.A. Weiss, Epidermal growth factor receptor (EGFR) and EGFRvIII in glioblastoma (GBM): signaling pathways and targeted therapies, Oncogene. 37 (2018) 1561–1575. https://doi.org/10.1038/s41388-017-0045-7.

[6] H. Xu, H. Zong, C. Ma, X. Ming, M. Shang, K. Li, X. He, H. Du, L. Cao, Epidermal growth factor receptor in glioblastoma, Oncol. Lett. 14 (2017) 512–516. https://doi.org/10.3892/ol.2017.6221.

[7] B. Hasselbalch, U. Lassen, S. Hansen, M. Holmberg, M. Sørensen, M. Kosteljanetz, H. Broholm, M.-T. Stockhausen, H.S. Poulsen, Cetuximab, bevacizumab, and irinotecan for patients with primary glioblastoma and progression after radiation therapy and temozolomide: a phase II trial, Neuro-Oncol. 12 (2010) 508–516. https://doi.org/10.1093/neuonc/nop063.

[8] B. Neyns, J. Sadones, E. Joosens, F. Bouttens, L. Verbeke, J.-F. Baurain, L. D'Hondt, T. Strauven, C. Chaskis, P. In't Veld, A. Michotte, J. De Greve, Stratified phase II trial of cetuximab in patients with recurrent high-grade glioma, Ann. Oncol. 20 (2009) 1596–1603. https://doi.org/10.1093/annonc/mdp032.

[9] U.H. Weidle, J. Niewöhner, G. Tiefenthaler, The Blood–Brain Barrier Challenge for the Treatment of Brain Cancer, Secondary Brain Metastases, and Neurological Diseases, Cancer Genomics - Proteomics. 12 (2015) 167–177.

[10] J. Jászai, M.H.H. Schmidt, Trends and Challenges in Tumor Anti-Angiogenic Therapies, Cells. 8 (2019). https://doi.org/10.3390/cells8091102.

[11] O. van Tellingen, B. Yetkin-Arik, M.C. de Gooijer, P. Wesseling, T. Wurdinger, H.E. de Vries, Overcoming the blood-brain tumor barrier for effective glioblastoma treatment, Drug Resist. Updat. Rev. Comment. Antimicrob. Anticancer Chemother. 19 (2015) 1–12. https://doi.org/10.1016/j.drup.2015.02.002.

[12] C.D. Arvanitis, G.B. Ferraro, R.K. Jain, The blood–brain barrier and blood–tumour barrier in brain tumours and metastases, Nat. Rev. Cancer. 20 (2020) 26–41. https://doi.org/10.1038/s41568-019-0205-x.

[13] A. D'Alessio, G. Proietti, G. Sica, B.M. Scicchitano, Pathological and Molecular Features of Glioblastoma and Its Peritumoral Tissue, Cancers. 11 (2019). https://doi.org/10.3390/cancers11040469.

[14] W.G. Lesniak, C. Chu, A. Jablonska, Y. Du, M.G. Pomper, P. Walczak, M. Janowski, PET imaging of intra-arterial 89Zr bevacizumab in mice with and without osmotic opening of the blood-brain barrier: distinct advantage of intra-arterial delivery, J. Nucl. Med. (2018) jnumed.118.218792. https://doi.org/10.2967/jnumed.118.218792.

[15] K. Hynynen, N. McDannold, N. Vykhodtseva, F.A. Jolesz, Noninvasive MR Imaging–guided Focal Opening of the Blood-Brain Barrier in Rabbits, Radiology. 220 (2001) 640–646. https://doi.org/10.1148/radiol.2202001804.
[16] E.E. Konofagou, Y.-S. Tunga, J. Choia, T. Deffieuxa, B.B. and F. Vlachosa, Ultrasound-Induced Blood-Brain Barrier Opening, Curr. Pharm. Biotechnol. (2012). http://www.eurekaselect.com/97989/article (accessed June 23, 2020).
[17] T. Mainprize, N. Lipsman, Y. Huang, Y. Meng, A. Bethune, S. Ironside, C. Heyn, R. Alkins, M. Trudeau, A. Sahgal, J. Perry, K. Hynynen, Blood-Brain Barrier Opening in Primary Brain Tumors with Non-invasive MR-Guided Focused Ultrasound: A Clinical Safety and Feasibility Study, Sci. Rep. 9 (2019) 1–7. https://doi.org/10.1038/s41598-018-36340-0.
[18] N. McDannold, N. Vykhodtseva, K. Hynynen, Targeted disruption of the blood-brain barrier with focused ultrasound: association with cavitation activity, Phys. Med. Biol. 51 (2006) 793–807. https://doi.org/10.1088/0031-9155/51/4/003.
[19] C.D. Arvanitis, V. Askoxylakis, Y. Guo, M. Datta, J. Kloepper, G.B. Ferraro, M.O. Bernabeu, D. Fukumura, N. McDannold, R.K. Jain, Mechanisms of enhanced drug delivery in brain metastases with focused ultrasound-induced blood-tumor barrier disruption, Proc. Natl. Acad. Sci. U. S. A. 115 (2018) E8717–E8726. https://doi.org/10.1073/pnas.1807105115.
[20] K.-T. Chen, K.-C. Wei, H.-L. Liu, Theranostic Strategy of Focused Ultrasound Induced Blood-Brain Barrier Opening for CNS Disease Treatment, Front. Pharmacol. 10 (2019). https://doi.org/10.3389/fphar.2019.00086.
[21] H.-L. Liu, P.-H. Hsu, C.-Y. Lin, C.-W. Huang, W.-Y. Chai, P.-C. Chu, C.-Y. Huang, P.-Y. Chen, L.-Y. Yang, J.S. Kuo, K.-C. Wei, Focused Ultrasound Enhances Central Nervous System Delivery of Bevacizumab for Malignant Glioma Treatment, Radiology. 281 (2016) 99–108. https://doi.org/10.1148/radiol.2016152444.
[22] M.J.W.D. Vosjan, L.R. Perk, G.W.M. Visser, M. Budde, P. Jurek, G.E. Kiefer, G.A.M.S. van Dongen, Conjugation and radiolabeling of monoclonal antibodies with zirconium-89 for PET imaging using the bifunctional chelate p-isothiocyanatobenzyl-desferrioxamine, Nat. Protoc. 5 (2010) 739–743. https://doi.org/10.1038/nprot.2010.13.
[23] T. Lindmo, E. Boven, F. Cuttitta, P.A. Bunn, Determination of the Immunoreactive Fraction of Radiolabeled Monoclonal Antibodies by Linear Extrapolation to Binding at Infinite Antigen Excess, (n.d.) 13.
[24] J.J. Choi, M. Pernot, S.A. Small, E.E. Konofagou, Noninvasive, transcranial and localized opening of the blood-brain barrier using focused ultrasound in mice, Ultrasound Med. Biol. 33 (2007) 95–104. https://doi.org/10.1016/j.ultrasmedbio.2006.07.018.
[25] M. Gerstenmayer, Ultrasound Induced Blood-brain Barrier Opening on Rodents : from Nanoparticles Delivery to a Therapy for Alzheimer's Disease, theses.fr, University Paris-Saclay (ComUE) , 2018.
[26] J. Logan, Graphical analysis of PET data applied to reversible and irreversible tracers, Nucl. Med. Biol. 27 (2000) 661–670. https://doi.org/10.1016/s0969-8051(00)00137-2.
[27] S. Auvity, H. Chapy, S. Goutal, F. Caillé, B. Hosten, M. Smirnova, X. Declèves, N. Tournier, S. Cisternino, Diphenhydramine as a selective probe to study H+-antiporter function at the blood–brain barrier: Application to [11C]diphenhydramine positron emission tomography imaging, J. Cereb. Blood Flow Metab. 37 (2017) 2185–2195. https://doi.org/10.1177/0271678X16662042.
[28] B. Vincenzi, G. Schiavon, M. Silletta, D. Santini, G. Tonini, The biological properties of cetuximab, Crit. Rev. Oncol. Hematol. 68 (2008) 93–106. https://doi.org/10.1016/j.critrevonc.2008.07.006.
[29] N. Ledón, A. Casacó, E. Casanova, I. Beausoleil, Comparative analysis of binding affinities to epidermal growth factor receptor of monoclonal antibodies nimotuzumab and cetuximab using different experimental animal models, Placenta. 32 (2011) 531–534. https://doi.org/10.1016/j.placenta.2011.04.008.
[30] M. Fumita, Robert, B. Innis, In vivo molecular imaging: ligand development and research applications, in: Neuropsychopharmacol. Fifth Gener. Prog., 2000: pp. 411–425.

637 [31] P. Wee, Z. Wang, Epidermal Growth Factor Receptor Cell Proliferation Signaling Pathways,
638 Cancers. 9 (2017). https://doi.org/10.3390/cancers9050052.
639 [32] M. Westphal, C.L. Maire, K. Lamszus, EGFR as a Target for Glioblastoma Treatment: An
640 Unfulfilled Promise, CNS Drugs. 31 (2017) 723–735. https://doi.org/10.1007/s40263-017-0456-
641 6.
642 [33] C. von Achenbach, M. Weller, E. Szabo, Epidermal growth factor receptor and ligand family
643 expression and activity in glioblastoma, J. Neurochem. 147 (2018) 99–109.
644 https://doi.org/10.1111/jnc.14538.
645 [34] L.G. Dubois, L. Campanati, C. Righy, I. D'Andrea-Meira, T.C.L. de S. e Spohr, I. Porto-Carreiro,
646 C.M. Pereira, J. Balça-Silva, S.A. Kahn, M.F. DosSantos, M. de A.R. Oliveira, A. Ximenes-da-Silva,
647 M.C. Lopes, E. Faveret, E.L. Gasparetto, V. Moura-Neto, Gliomas and the vascular fragility of the
648 blood brain barrier, Front. Cell. Neurosci. 8 (2014). https://doi.org/10.3389/fncel.2014.00418.
649 [35] V. Neves, F. Aires-da-Silva, S. Corte-Real, M.A.R.B. Castanho, Antibody Approaches To Treat
650 Brain Diseases, Trends Biotechnol. 34 (2016) 36–48.
651 https://doi.org/10.1016/j.tibtech.2015.10.005.
652 [36] A. Khaibullina, B.-S. Jang, H. Sun, N. Le, S. Yu, V. Frenkel, J.A. Carrasquillo, I. Pastan, K.C.P. Li,
653 C.H. Paik, Pulsed high-intensity focused ultrasound enhances uptake of radiolabeled
654 monoclonal antibody to human epidermoid tumor in nude mice, J. Nucl. Med. Off. Publ. Soc.
655 Nucl. Med. 49 (2008) 295–302. https://doi.org/10.2967/jnumed.107.046888.
656 [37] K.-T. Chen, K.-C. Wei, H.-L. Liu, Theranostic Strategy of Focused Ultrasound Induced Blood-Brain
657 Barrier Opening for CNS Disease Treatment, Front. Pharmacol. 10 (2019).
658 https://doi.org/10.3389/fphar.2019.00086.
659 [38] P.W. Janowicz, G. Leinenga, J. Götz, R.M. Nisbet, Ultrasound-mediated blood-brain barrier
660 opening enhances delivery of therapeutically relevant formats of a tau-specific antibody, Sci.
661 Rep. 9 (2019) 9255. https://doi.org/10.1038/s41598-019-45577-2.
662 [39] F. Bensch, E.L. van der Veen, M.N.L. Hooge, A. Jorritsma-Smit, R. Boellaard, I.C. Kok, S.F.
663 Oosting, C.P. Schröder, T.J.N. Hiltermann, A.J. van der Wekken, H.J.M. Groen, T.C. Kwee, S.G.
664 Elias, J.A. Gietema, S.S. Bohorquez, A. de Crespigny, S.-P. Williams, C. Mancao, A.H. Brouwers,
665 B.M. Fine, E.G.E. de Vries, 89 Zr-atezolizumab imaging as a non-invasive approach to assess
666 clinical response to PD-L1 blockade in cancer, Nat. Med. 24 (2018) 1852.
667 https://doi.org/10.1038/s41591-018-0255-8.
668 [40] A.N. Niemeijer, D. Leung, M.C. Huisman, I. Bahce, O.S. Hoekstra, G.A.M.S. van Dongen, R.
669 Boellaard, S. Du, W. Hayes, R. Smith, A.D. Windhorst, N.H. Hendrikse, A. Poot, D.J. Vugts, E.
670 Thunnissen, P. Morin, D. Lipovsek, D.J. Donnelly, S.J. Bonacorsi, L.M. Velasquez, T.D. de Gruijl,
671 E.F. Smit, A.J. de Langen, Whole body PD-1 and PD-L1 positron emission tomography in patients
672 with non-small-cell lung cancer, Nat. Commun. 9 (2018) 4664. https://doi.org/10.1038/s41467-
673 018-07131-y.
674 [41] C. Estrada, A. Villalobo, Epidermal Growth Factor Receptor in the Adult Brain, in: D. Janigro
675 (Ed.), Cell Cycle Cent. Nerv. Syst., Humana Press, Totowa, NJ, 2006: pp. 265–277.
676 https://doi.org/10.1007/978-1-59745-021-8_20.
677 [42] B.A.W. Hoeben, J.D.M. Molkenboer-Kuenen, W.J.G. Oyen, W.J.M. Peeters, J.H.A.M. Kaanders, J.
678 Bussink, O.C. Boerman, Radiolabeled cetuximab: Dose optimization for epidermal growth factor
679 receptor imaging in a head-and-neck squamous cell carcinoma model, Int. J. Cancer. 129 (2011)
680 870–878. https://doi.org/10.1002/ijc.25727.
681 [43] N.J. Abbott, Dynamics of CNS barriers: evolution, differentiation, and modulation, Cell. Mol.
682 Neurobiol. 25 (2005) 5–23. https://doi.org/10.1007/s10571-004-1374-y.
683 [44] A.-M. Chacko, C. Li, D.A. Pryma, S. Brem, G. Coukos, V.R. Muzykantov, Targeted delivery of
684 antibody-based therapeutic and imaging agents to CNS tumors: Crossing the blood-brain-
685 barrier divide, Expert Opin. Drug Deliv. 10 (2013) 907–926.
686 https://doi.org/10.1517/17425247.2013.808184.
687 [45] A. Conti, R. Magnin, M. Gerstenmayer, N. Tsapis, E. Dumont, O. Tillement, F. Lux, D. Le Bihan, S.
688 Mériaux, S. Della Penna, B. Larrat, Empirical and Theoretical Characterization of the Diffusion

689 Process of Different Gadolinium-Based Nanoparticles within the Brain Tissue after Ultrasound-
690 Induced Permeabilization of the Blood-Brain Barrier, Contrast Media X26 Mol. Imaging. (2019).
691 https://doi.org/10.1155/2019/6341545.
692 [46] S. Goutal, M. Gerstenmayer, S. Auvity, F. Caillé, S. Mériaux, I. Buvat, B. Larrat, N. Tournier,
693 Physical blood-brain barrier disruption induced by focused ultrasound does not overcome the
694 transporter-mediated efflux of erlotinib, J. Control. Release Off. J. Control. Release Soc. 292
695 (2018) 210–220. https://doi.org/10.1016/j.jconrel.2018.11.009.
696 [47] E.D. Lobo, R.J. Hansen, J.P. Balthasar, Antibody Pharmacokinetics and Pharmacodynamics, J.
697 Pharm. Sci. 93 (2004) 2645–2668. https://doi.org/10.1002/jps.20178.
698 [48] D.K. Shah, A.M. Betts, Antibody biodistribution coefficients, MAbs. 5 (2013) 297–305.
699 https://doi.org/10.4161/mabs.23684.
700 [49] P.R. Cooper, G.J. Ciambrone, C.M. Kliwinski, E. Maze, L. Johnson, Q. Li, Y. Feng, P.J. Hornby,
701 Efflux of monoclonal antibodies from rat brain by neonatal Fc receptor, FcRn, Brain Res. 1534
702 (2013) 13–21. https://doi.org/10.1016/j.brainres.2013.08.035.
703 [50] D.J. Wolak, M.E. Pizzo, R.G. Thorne, Probing the extracellular diffusion of antibodies in brain
704 using in vivo integrative optical imaging and ex vivo fluorescence imaging, J. Control. Release
705 Off. J. Control. Release Soc. 0 (2015) 78–86. https://doi.org/10.1016/j.jconrel.2014.10.034.
706 [51] J. Silburt, N. Lipsman, I. Aubert, Disrupting the blood–brain barrier with focused ultrasound:
707 Perspectives on inflammation and regeneration, Proc. Natl. Acad. Sci. U. S. A. 114 (2017)
708 E6735–E6736. https://doi.org/10.1073/pnas.1710761114.
709